

# Bulk motion of granular matter in an agitated cylindrical bed

Phanikumar Sistla,<sup>1</sup> Oleh Baran,<sup>2</sup> Q. Chen,<sup>1</sup> Peter H. Poole,<sup>2,3</sup> and Robert J. Martinuzzi<sup>1</sup>

<sup>1</sup>*Department of Mechanical and Materials Engineering,*

*University of Western Ontario, London, Ontario N6A 5B9, Canada*

<sup>2</sup>*Department of Applied Mathematics, University of Western Ontario, London, Ontario N6A 5B7, Canada*

<sup>3</sup>*Department of Physics, St. Francis Xavier University, Antigonish, Nova Scotia B2G 2W5, Canada*

(Dated: February 1, 2008)

Experimental results are reported for the bulk motion induced in a bed of granular matter contained in a cylindrical pan with a flat bottom subjected to simultaneous vertical and horizontal vibrations. The motion in space of the moving pan is quantified. A number of distinct bulk dynamical modes are observed in which the particle bed adopts different shapes and motions. At the lowest pan excitation frequency  $\omega$ , the bed forms a “heap,” and rotates about the cylinder axis. As  $\omega$  is increased, a more complex “toroidal” mode appears in which the bed takes the shape of a torus; in this mode, circulation occurs both about the cylinder axis, and also radially, with particles moving from the outer edge of the pan to the centre on the top surface of the bed, and back to the outer edge along the pan bottom. At the highest  $\omega$ , surface modulations (“surface waves” and “sectors”) of the toroidal mode occur. The origin of this family of behavior in terms of the pan motion is discussed.

## I. INTRODUCTION

Granular materials play an important role in many industrial processes. In applications, granular materials are often subjected to vibrations to generate material transport, mixing, or size segregation. Consequently, the fundamental properties and motions of granular matter confined to a vibrating container have been widely studied. Many fundamental studies have focused on the motion of particle beds in a rectangular container (the pan). Typically, the bed is excited by pan vibrations along a single axis. Reviews of such studies can be found in Refs. [1, 2, 3, 4, 5, 6]. Agitated beds of granular matter have been observed to adopt a wide spectrum of shapes and motions, such as heaping, convection, small amplitude wave motion, arching, and large amplitude wave motion; see e.g. Ref. [7]. These modes certainly depend on the nature of the vibrations. However, their dependence on the pan geometry is less well understood. For example, in the case of purely vertical vibrations, the effect of the pan shape is absent or weak [8], but this is unlikely to be generally true in the presence of horizontal vibrations.

The motions observed in a cylindrical pan subjected to simultaneous horizontal and vertical vibrations, are reported in the present study. There are two principal motivations for studying this case. First, the response of a bed of granular matter to excitations occurring simultaneously along three Cartesian axes has not been extensively studied and remains poorly understood. However, in many industrial applications, tri-axial excitations are highly desirable to optimize process parameters. Many fundamental studies have been made of systems subjected to purely vertical or horizontal vibrations, but in only a few cases are vibrations in both directions addressed. An example is the work of Tennekoon and Behringer [9], who reported that when granular matter is subjected to simultaneous horizontal and vertical sinu-

soidal vibrations, the phase difference between the components of vibration in the two directions becomes a key control parameter for the resulting motion. A quantitative understanding of the effect of such combined vibrations is therefore important for predicting and controlling the behavior of agitated beds in real applications.

A second motivation is to study the motion generated in a container of cylindrical symmetry, with the cylinder axis oriented vertically. Again, this geometry is common in industrial devices such as sifting machinery, yet is less well studied in a research context compared to square and rectangular geometries. Note that the present case is distinct, both in motion and in orientation, from the more widely studied case of a continuously rotating drum having the cylinder axis oriented horizontally.

A cylindrical geometry provides the opportunity to study phenomena unlikely to occur in the rectangular case. In particular, the absence of discontinuities (i.e. sharp corners) on the vertical boundaries of a cylindrical pan makes possible smooth circulatory motions of the agitated bed. These circulation modes are of interest for applications involving sifting and mixing, and for developing agitated bed devices for continuous, as opposed to batch, processing. Initial studies have also demonstrated that these modes may display complex behavior. For example, Scherer et al. [10] have reported that when spheres are placed in a cylindrical pan and are subjected to horizontal shaking, they circulate in one direction at low packing densities, and in the other at high packing densities or high excitation frequencies.

## II. EXPERIMENTAL SET-UP

The agitated bed apparatus studied here (Figs. 1 and 2) is a modified SWECO finishing mill Model ZS30S66, a commercially available device widely used in industrial applications for sieving and polishing. It consists of a

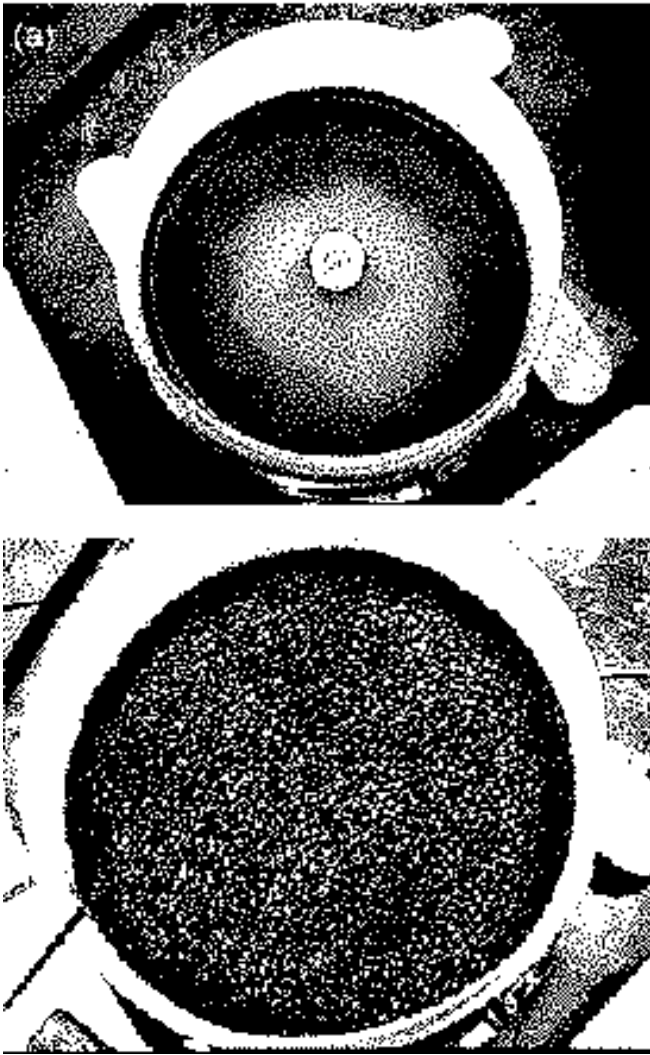


FIG. 1: Photographs of the agitated bed apparatus, viewed from above: (a) without particles; (b) with particles.

rigid, circular, stainless steel pan of radius  $R = 0.381$  m with a flat bottom. The pan “floats” on an array of nine springs spaced equidistantly around the circumference of the pan bottom. Vibrations are excited by a 0.5 HP motor mounted below the center of the pan.

In order to induce simultaneous horizontal and vertical vibrations, and concurrently obtain control over their relative magnitudes, metal weights are mounted eccentrically at the top and bottom ends of a shaft running through the center of the motor. The motor housing is rigidly attached to the pan via a flange, while the shaft rotates freely with respect to the pan. When the shaft rotates, the effect of the weights is to impose an oscillatory torque that tends to make the motor shaft deviate from the vertical. The affect of this torque is to cause the center of the pan to revolve about a vertical axis, and simultaneously cause the bottom of the pan to deviate from the horizontal. A complete description of the pan motion is given in the next section. The angle between

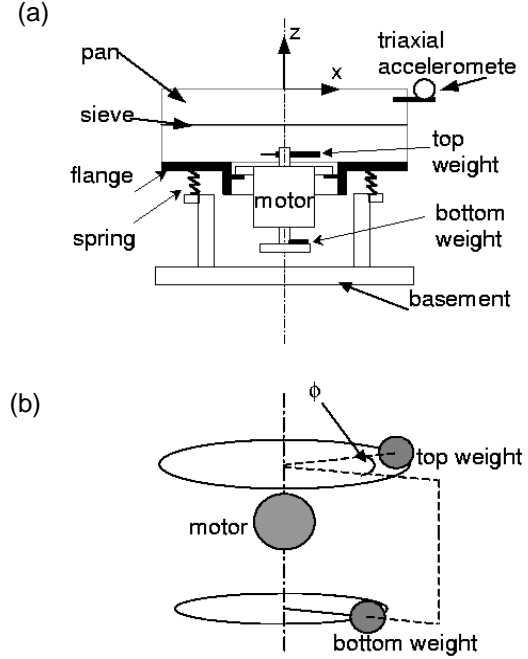


FIG. 2: (a) A schematic view of the apparatus. (b) Schematic representation of the relative positions of the motor and top and bottom weights, and the definition of  $\phi$ .

the top and bottom weights, referred to here as the “lead angle”  $\phi$ , can be varied from  $0^\circ$  to  $180^\circ$  [Fig. 2(b)]. The motor shaft rotates the weights in a range of frequency  $\omega$  of 10 to 20 Hz.

The bottom surface of the pan is a stiff, stainless steel sieve. The particles used in this study are too large to fall through the holes of the sieve. The springs that bear the load of the entire pan-motor assembly are mounted on a rigid basement. Note also that there is a cylindrical “hub” attached to the center of the pan bottom, of radius 10.4 cm and height 3.0 cm.

The masses of the top and bottom weights attached to the motor are fixed in this study. As will be shown in the next section, the angle  $\phi$  between the weights controls the ratio of the amplitudes of the horizontal and vertical vibrations imparted to the pan. The rotational frequency  $\omega$  of the motor controls the amount of energy introduced into the system. The principal control parameters for the experiments described here are thus  $\phi$  and  $\omega$ .

The experiments are conducted with two sets particles: “pill-shaped” oblate spheroid particles, and spherical particles. The oblate spheroids have a major axis of 13.5 mm and a minor axis of 7 mm, a mass of 0.9 g and a density of  $1200 \text{ kg/m}^3$ , with a hard and smooth polished surface. The spheres have the same volume as the oblate

spheroids, a density of  $1100 \text{ kg/m}^3$ , and a hard, smooth but unpolished surface. Although the qualitative behavior observed in both cases is similar, it is found that the shape of the particles influences some quantitative properties of the motion. Thus the results obtained with each type of particle are presented separately.

The mass of the unloaded pan is approximately 150 kg. All tests are conducted for particle bed loads below 45 kg and it is found that the influence of the bed load on the pan motion is negligible. Also, it is confirmed in all tests that the pan moves as a rigid body.

The motion of the pan is monitored using Entran accelerometers: one tri-axial (model EGA3-F-10-/5) and three mono-axial (model EGA-F-10-/5) units are used. The location of the tri-axial accelerometer is shown in Fig. 2; the others are positioned at various locations along the top edge of the pan, according to the degree of freedom to be measured. The accelerometer data are collected using a computer-based data acquisition system and processed to obtain the velocity, displacement and phase-shift data for the pan motion. A sampling frequency of 2 kHz is used for data acquisition, allowing a minimum resolution of 165 points/cycle. This results in an error in the phase angle measurements of  $\pm 3^\circ$ . The uncertainty in the acceleration and bed displacement are estimated to be  $\pm 0.1 \text{ g}$  and  $\pm 0.05 \text{ mm}$ , respectively, where  $g$  is the acceleration due to gravity.

The surface motion of the particle bed is studied by visually tracking particles. Differently colored particles are used to obtain information on the average mixing time. For the most interesting modes of motion, a localized group of particles is coated with a fluorescent dye and the subsequent motion of this group is recorded photographically. The dye is sodium fluoresceine, which is excited using an ultra-violet light source and observed in the 532 nm visual range.

The results of the experiments are presented in two stages. First, a quantification of the pan motion is presented in Section 3. Then the modes of particle motion that are observed in the bed are described in Section 4.

### III. PAN MOTION

As described above, the experimental apparatus is a commercially available unit that generates simultaneous horizontal and vertical vibrations of the pan. The first task of the present study is therefore to quantify the motion generated by this device. To achieve this, two coordinate systems are defined: one fixed with respect to the pan (the “pan frame”), and one fixed with respect to the laboratory (the “lab frame”).

The intersection of the cylinder axis of the pan with the plane defined by the top edge of the pan is chosen as the origin of the Cartesian coordinate system  $(x_p, y_p, z_p)$  fixed in the pan frame. The cylindrical symmetry of the pan is broken by the existence of a spout located at a point on the circumference of the pan. The  $x_p$ -axis in the

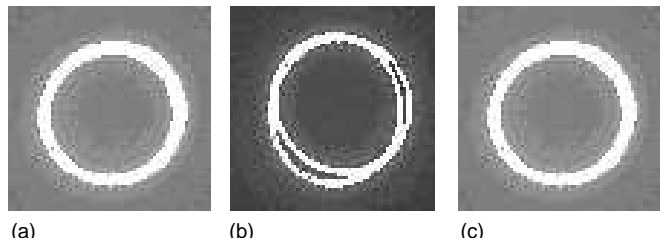


FIG. 3: Photographs of laser traces visualizing the circular motion of the pan center for (a)  $\phi = 10^\circ$ ,  $\omega = 30 \text{ Hz}$ ; (b)  $\phi = 60^\circ$ ,  $\omega = 30 \text{ Hz}$ ; and (c)  $\phi = 100^\circ$ ,  $\omega = 30 \text{ Hz}$ .

pan frame is thus defined as the line that passes through the origin and the location on the spout where the tri-axial accelerometer is mounted. The  $y_p$ -axis is the line perpendicular to the  $x_p$ -axis in the plane defined by the top edge of the pan, and the  $z_p$ -axis is perpendicular to both the  $x_p$  and  $y_p$ -axes. The Cartesian coordinate system  $(x, y, z)$  in the lab frame is defined as that which is coincident with the pan frame when the apparatus is at rest.

The accelerometers provide data that are analyzed to give the lab frame coordinates as a function of time for points fixed in the pan frame. To specify the motion of the pan, in the following attention is restricted to points fixed in the pan frame lying in the  $z_p = 0$  plane, since this is the plane in which the accelerometers are located. Based on the accelerometer data, the motion in the lab frame of such a point is found to be consistent, within the error of measurement, with the following model:

$$x(t) = x_p + x_{\max} \cos(\omega t) \quad (1)$$

$$y(t) = y_p + y_{\max} \cos(\omega t + \alpha_{xy}) \quad (2)$$

$$z(t) = A(r_p) \cos(\omega t + \alpha_{xz} - \theta), \quad (3)$$

where,

$$A(r_p) = \frac{r_p}{R} z_{\max}, \quad (4)$$

and

$$r_p = \sqrt{x_p^2 + y_p^2}. \quad (5)$$

In the above equations,  $x_{\max}$  and  $y_{\max}$  are the amplitudes of the  $x$  and  $y$  displacements of the pan-frame origin in the lab frame;  $\alpha_{xy}$  is the phase shift between the  $x$  and  $y$  displacements in the lab frame; and  $\theta$  is the angle measured about the origin from the  $x_p$ -axis to the point  $(x_p, y_p)$ .  $\alpha_{xz}$  is the phase shift between the  $x$  and  $z$  displacements in the lab frame, as measured on the  $x_p$ -axis; thus  $(\alpha_{xz} - \theta)$  is the phase shift between the  $x$  and  $z$  displacements in the lab frame, to be found at the point  $(x_p, y_p)$ .  $A(r_p)$  is the amplitude of the  $z$  displacement of a point in the  $z_p = 0$  plane that is a distance  $r_p$  from the origin in the pan frame.  $R = 0.381 \text{ m}$  is the distance from the origin in the pan frame to the edge of the pan, and  $z_{\max}$  is the amplitude of the  $z$  displacement of a point on the edge of the pan (i.e. at  $r_p = R$ ).

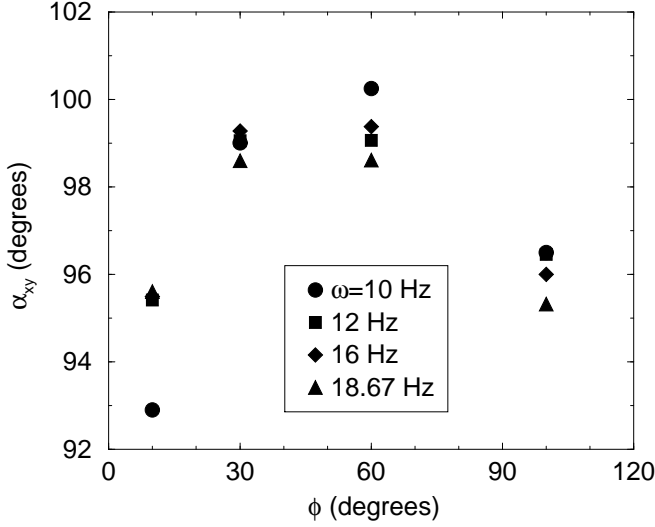


FIG. 4: Phase shift  $\alpha_{xy}$  as a function of  $\phi$  for various  $\omega$

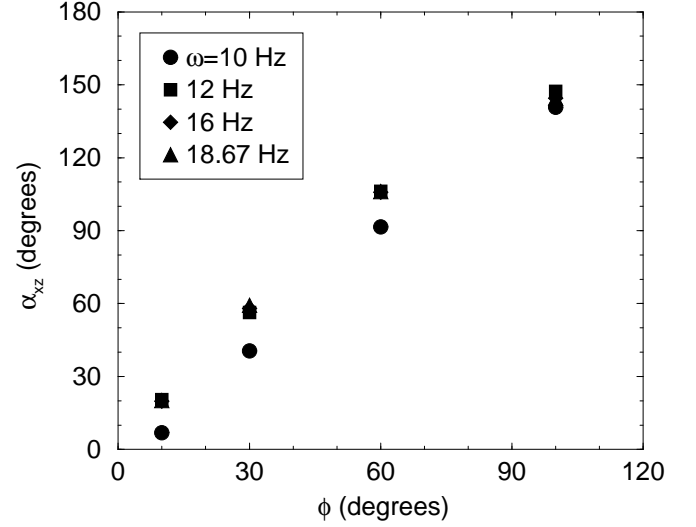


FIG. 6: Phase shift  $\alpha_{xz}$ , as a function of  $\phi$  for various  $\omega$ .

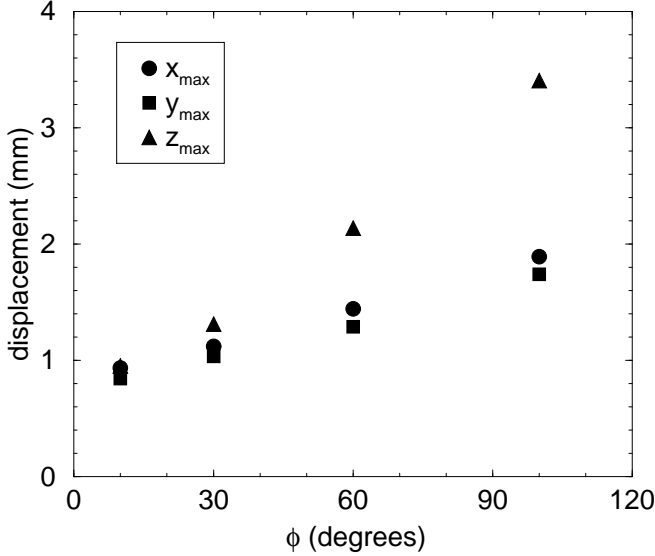


FIG. 5: Maximum displacements  $x_{\max}$ ,  $y_{\max}$  and  $z_{\max}$  as a function of  $\phi$ . These data are averages over approximately 20 runs over the range of  $\omega$  studied. No systematic variation is observed as a function of  $\omega$ , though individual measurements are scattered about the average by about 15%.

The form of Eqs. 1 and 2 is motivated by the observation that under all operating conditions, the center of the pan appears to execute an approximately circular orbit in a horizontal plane. To visualize this, a laser source is mounted at the center of the pan, pointing upward, normal to the pan bottom. The motion of the pan causes the laser to trace out a pattern on a screen positioned horizontally above the apparatus. Time-exposure photographs of these traces are shown in Fig. 3 for various operating conditions, and are consistent with circular motion of the pan center.

If the motion is nearly circular, the magnitude of the phase shift  $\alpha_{xy}$  should be approximately  $90^\circ$ . This is confirmed in Fig. 4, where  $\alpha_{xy}$  is plotted as a function of  $\phi$  for various  $\omega$ . An apparatus with perfect cylindrical symmetry would have  $\alpha_{xy} = 90^\circ$ . Small asymmetries in the apparatus, the most important of which is likely the spout on the edge of the pan, result in the observed variation in the range  $93^\circ < \alpha_{xy} < 100^\circ$ .

Circular motion of the pan center also requires  $x_{\max}$  and  $y_{\max}$  to be equal. Measurements of  $x_{\max}$  and  $y_{\max}$  at  $r_p = R$  (Fig. 5) show that this is observed to be true within the measurement error across the range of  $\phi$  studied here. Note that as  $\omega$  varies in different test runs,  $x_{\max}$  and  $y_{\max}$  are found to be scattered around the average values reported in Fig. 5 by about 15%; however, no systematic variation with  $\omega$  can be identified. Tests also show that the values of  $x_{\max}$  and  $y_{\max}$  are independent of the position around the edge of the pan at  $r_p = R$  at which they are measured, consistent with the description in Eqs. 1 and 2. Note that for  $x_{\max}$  or  $y_{\max}$  to have the same measured value independent of  $r_p$  at the point of measurement requires that the tilt angle of the  $z_p = 0$  plane with respect to the  $z = 0$  plane be small. This is confirmed below.

Eq. 3 characterizes the tilting motion of the pan by quantifying the vertical deviation of a point fixed in the pan frame (in the  $z_p = 0$  plane) with respect to the  $z = 0$  plane in the lab frame. As in the case of the  $x$  and  $y$  motions, the accelerometer data for  $z(t)$  indicate a sinusoidal function of  $t$ . The form of Eq. 3 also assumes that the origin of the pan frame does not leave the  $z = 0$  plane of the lab frame; this assumption is confirmed by direct visual observation using a high-speed (500 frames/s) camera. From geometric considerations, the amplitude  $A$  of the  $z$  variation in Eq. 3 is a function of the distance  $r_p$  of the point of measurement from the center of the pan, as indicated in Eq. 4. The phase shift between the  $x$  and

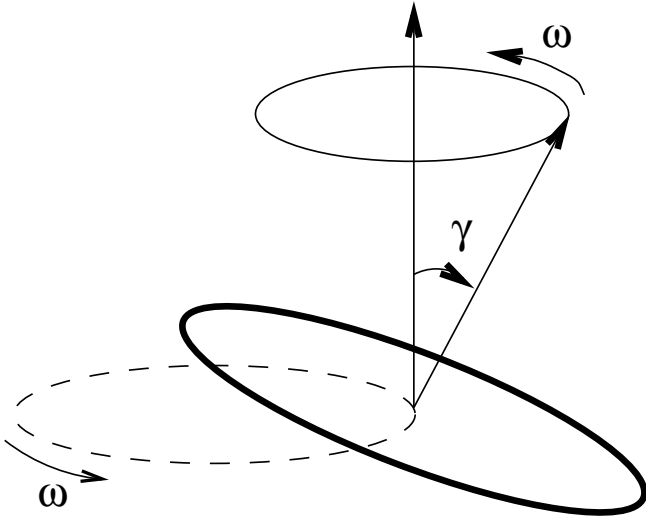


FIG. 7: Schematic representation of the pan motion. The dashed circle represents the orbit of the pan centre in the lab frame. The solid circle represents the rim of the pan.

$z$  displacements is a difference of two contributions,  $\alpha_{xz}$  and  $\theta$ .  $\alpha_{xz}$  is the phase shift between the  $x$  and  $z$  displacements as measured on the  $x_p$  axis at  $r_p = R$ .  $\theta$  is a geometrical term that accounts for the difference between the phase shift observed on the  $x_p$  axis and that which would be observed at an arbitrary point  $(x_p, y_p)$  in the  $z_p = 0$  plane. As shown in Fig. 6,  $\alpha_{xz}$  does not depend strongly on  $\omega$ , but does depend on  $\phi$ .

The net effect of the motions described by Eqs. (1-3) are summarized in Fig. 7. The motion of the pan can be thought of as a superposition of two motions:

(i) The center of the pan revolves about the lab frame origin in a nearly circular, horizontal orbit. This motion is directly described by Eqs. (1-2).

(ii) The pan is tilted at an angle  $\gamma$  in such a way that a unit normal vector rooted at the pan center precesses about the vertical at the same frequency at which the center orbits the origin, but phase shifted with respect to the orbital motion of the center. The fact that  $\gamma$  maintains a constant value can be shown from Eq. (3) by considering (e.g.) the case  $r_p = R$  and setting  $\theta = \omega t + \alpha_{xz}$ . These conditions describe the point on the edge of the pan that at any given  $t$  has the largest positive  $z$  displacement. For all  $t$ , this displacement is a constant,  $z_{\max}$ , and so  $\gamma = \sin^{-1}(z_{\max}/R)$  is also constant. Note that for the apparatus and operating conditions described here,  $R = 0.381$  m, and  $z_{\max}$  is never greater than 0.0035 m, giving  $\gamma < 0.5^\circ$ . This confirms the assumption of small tilt angle required for the chosen form of Eqs. (1-2), as indicated above.

The measurements shown in Figs. 4-6 show that both the amplitudes and phase shifts required to specify the pan motion using Eqs. (1-3) are mainly controlled by  $\phi$ . The effect of  $\omega$  is less problematic, since the ratio of displacements  $x_{\max}$  and  $z_{\max}$  do not vary in a systematic

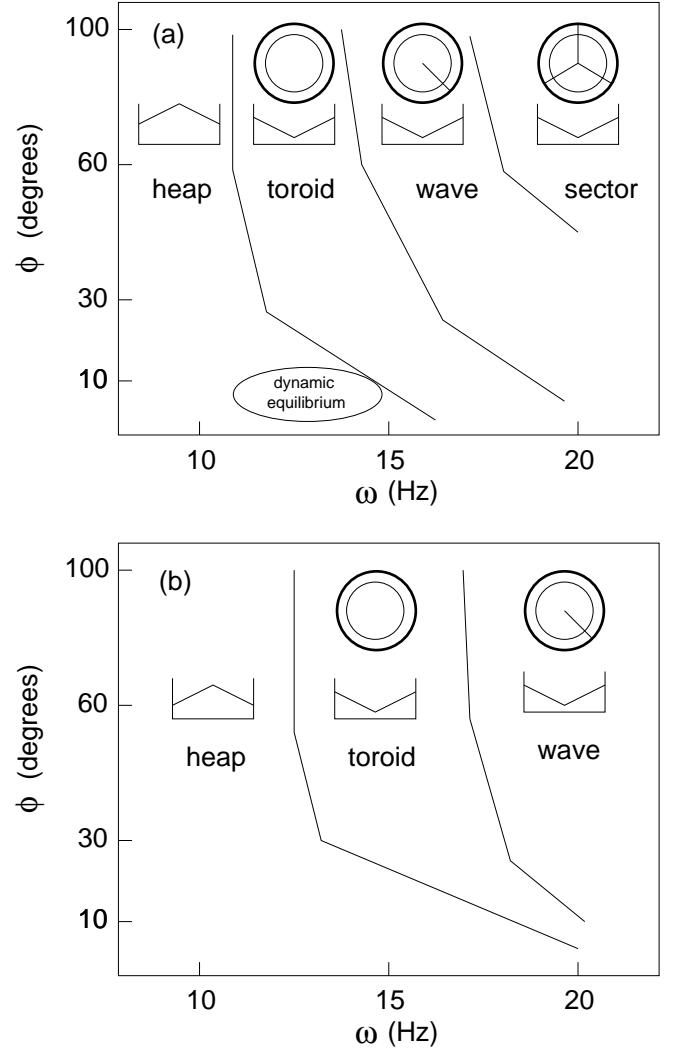


FIG. 8: Diagram identifying the regions of the  $\omega$ - $\phi$  plane in which distinct bulk dynamical modes of the particle bed are observed for (a) oblate spheroids, and (b) spheres. Note that in (a) a region of dynamic equilibrium is observed near  $\phi = 10^\circ$ , where the bed does not perform any net rotation about the pan centre. This is the boundary region between counter-clockwise and clockwise bed rotation (“laps”).

way with  $\omega$ . However, since  $\omega$  controls the rate at which energy is introduced into the system, both  $\phi$  and  $\omega$  will play a major role in determining the particle motion, as shown next.

#### IV. MODES OF PARTICLE BED MOTION

A diagram showing the observed bulk dynamical modes of the particle bed as a function of  $\omega$  and  $\phi$  is shown in Fig. 8(a) for the oblate spheroids, and in Fig. 8(b) for spheres. The bulk motion of the bed is a strong function of the  $\omega$ . Four distinct modes of bed motion are observed, here termed “heaping,” “toroidal

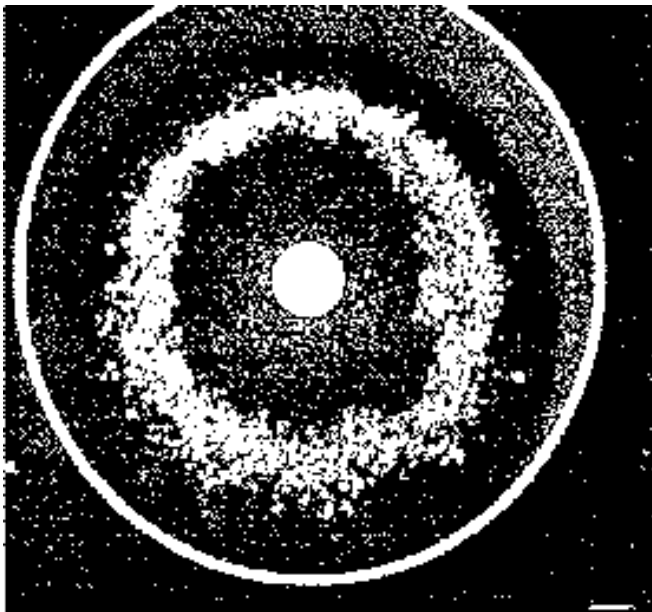


FIG. 9: Fluorescence dye visualization of the particle bed surface motion in the heaping mode. 30 kg,  $\phi = 60^\circ$ ,  $\omega = 30$  Hz.

motion,” “surface waves” and “sectors.” Each of these is described in detail below. The range of the  $\omega$  at which each of the modes appears depends on the particle shape as can be seen from Fig. 8, but the qualitative behavior of the modes is mostly similar. In the following sections, the motion in general is discussed, and differences due to particle shape are identified where appropriate.

### A. Heaping

At the lowest  $\omega$  studied the particles form a heap with an elevated center. The relative particle movement and mixing is very small and the particle bed rotates almost as a solid body. This motion is visualized in Fig. 9. Fluorescent dye is continuously added at a specific location to the surface of the particle bed while in steady-state motion. The subsequent motion of the dyed particles is then captured photographically under ultra-violet light, as shown in Fig. 9. The dyed particles on average undergo a slow proceSSIONAL motion about the pan center. The radial component of the particle motion and the diffusion of particles is negligible. Notably, for most  $\omega$  and  $\phi$ , the particle bed rotates in the direction opposite to that of the orbital motion of the center of the pan; the exceptions to this occur at the lowest  $\phi$  and  $\omega$  studied (e.g.  $\phi = 10^\circ$  and 16 Hz for oblate spheroids), where the rotational directions are the same. The direction of motion of the bed appears to depend on the phase difference  $\alpha_{yz} = \alpha_{xz} - \alpha_{xy}$ . For  $\alpha_{yz} > 0^\circ$ , the bed rotates in the direction opposite of the pan center.

The slope of the particle bed (from the center to the outer edge) increases with an increase in  $\phi$ . For example,

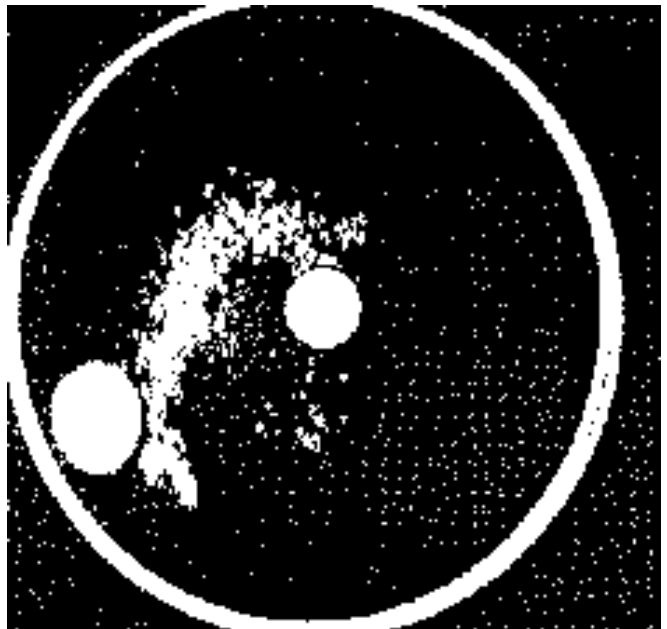


FIG. 10: Fluorescence dye visualization of the particle bed surface motion in the toroidal mode. Particles spiral to the center of the bed along the surface and toward the edges along the pan surface. These reappear at the surface of the bed along the edges. 30 kg,  $\phi = 60^\circ$ ,  $\omega = 56$  Hz.

the bed of oblate spheroids attains the maximum slope for  $\phi = 100^\circ$ , and a nearly flat surface when  $\phi = 10^\circ$ . Fig. 8 schematically shows the cross-sectional shape of the surface during the heaping mode.

The spherical particles move in more tightly packed layers than the oblate spheroids. For  $\phi = 100^\circ$ , the layers are very tightly packed and the local arrangement of particles is similar to a close-packed lattice. As  $\phi$  increases, the uniformity of the lattice breaks down. The bed is still tightly packed at  $\phi = 100^\circ$ , but more pronounced relative motion of the particles is observed. This change in behavior may be related to the increase of  $z_{\max}$  as  $\phi$  increases (see Fig. 5).

Previous studies of granular matter in vertically excited rectangular containers [12] have shown that relative particle motion is observed when the maximum vertical acceleration exceeds  $1.2g$ . In the present tests, it is found that the local acceleration is below this threshold for  $\omega < 10$  Hz. However, at  $\phi = 100^\circ$ , the acceleration at the edge of the pan does approach  $1.2g$ .

### B. Toroidal Motion

As  $\omega$  increases the particle bed undergoes a transformation to a toroidal shape and the particle motion becomes organized. This motion is highly coherent as seen in the fluorescent dye visualizations in Fig. 10. Dye is continuously injected onto the surface of the moving bed. Particles initially on the outer edge move in a spiral mo-

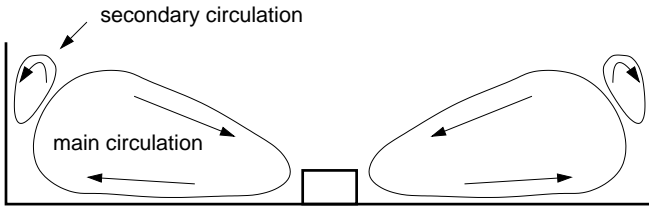


FIG. 11: Schematic of cross-section of particle bed, showing direction of particle flows in toroidal motion.

tion to the center. Near the center they are subducted and travel outward along the bottom of the pan, to be re-entrained along the walls and reappear at the surface at the outer edge of the pan. As seen for the heap, the bulk rotational motion of the bed in the horizontal plane is opposite to that of the center of the pan. The entire particle bed adopts the shape of a torus, through which individual particles move in helical trajectories. The particle motion in a cross-sectional plane through the toroid is depicted schematically in Fig. 11. Note that in addition to the primary circulation roll occupying the center portion of the bed, a small secondary (and counter-rotating) circulation roll forms on the top of the primary one, near the pan wall. The particles move toward the center along the top surface in the primary roll, and toward the wall along the top surface in the secondary roll. The slope of the particle bed surface is greater in magnitude, and opposite in sign, than that observed for the heap motion.

In this mode of motion, the particle bed is fluidized. The increased agitation results in a relatively rapid diffusion of the particles and a net increase in the mixing rate.

The toroidal motion observed for the circular pan has not been observed in rectangular geometries. An inward spiraling motion has been observed for granular media underneath rotating fluids [10] and the radial segregation of granular mixtures has been observed in rotating cylinders [11]. For vertically excited rectangular beds, stationary convection cells, similar to Rayleigh-Benard instabilities, are observed [12, 13]. For horizontal vibrations, experimental [14] and computational [15] studies have shown that the convective motion consists of granular matter rising to the surface at the middle of the container. In contrast, in the present study, the particles rise along the walls and are subducted at the middle of the pan.

### C. Surface Waves

For the two modes described above, the bed height is only a function of the distance from the center of the pan, and the shape of the bed is symmetric about the cylinder axis of the pan. However, for  $\omega > 15$  Hz, crests and troughs appear on the surface of the bed as a function of angular direction around the pan. The crests, or fronts, propagate in the same direction but at a higher speed

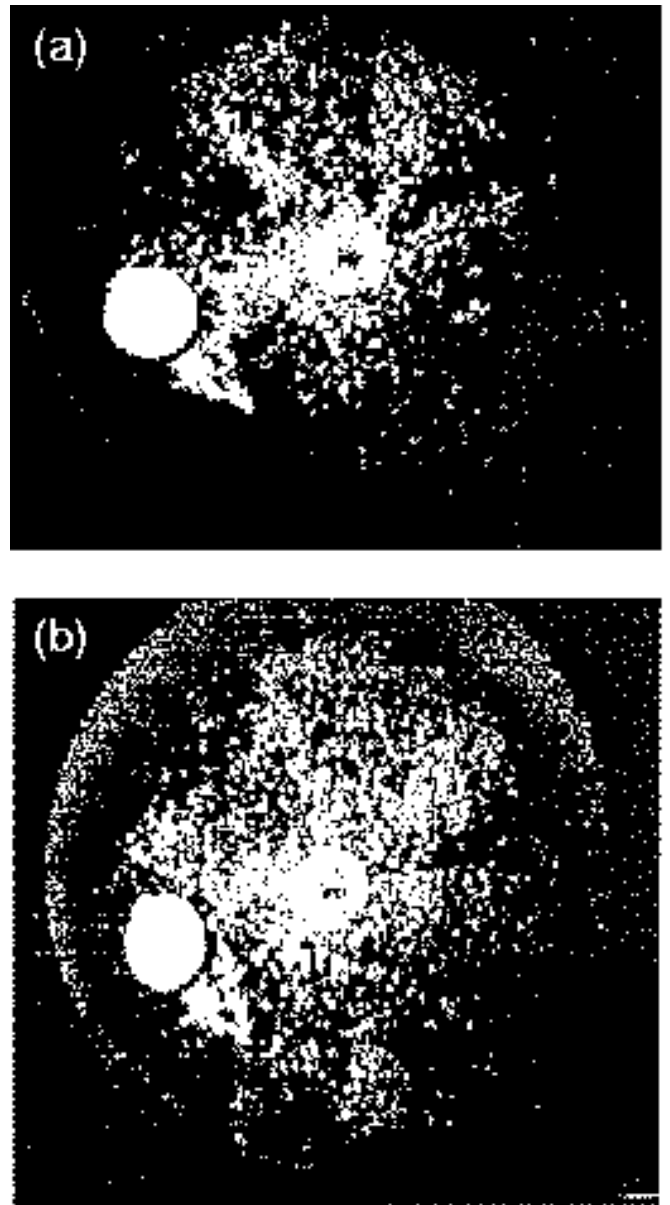


FIG. 12: Two fluorescence dye visualizations of sectors. The sectors can be visualized because the particles located on the crests dry faster than those in the trough and loose fluorescence.

than the bulk rotation of the bed in the horizontal plane. The speed of the particle fronts initially increases as  $\omega$  increases, but then decreases as  $\omega$  approaches 18 Hz. The amplitude (i.e. the height of the crest above the bed) decreases as  $\omega$  increases. Unfortunately, this motion is very difficult to capture on still media.

The individual particle trajectories can still be described as helical. The motion of the crests appears to be similar to a traveling wave.

### D. Sectors

For  $18 \text{ Hz} < \omega < 20 \text{ Hz}$ , the motion of crests on the surface of the bed becomes nearly stationary, dividing the bed into well-defined “sectors.” These sectors are visualized using fluorescent dye in Fig. 12. The number of sectors present in the bed is found to be a function of  $\phi$  and  $\omega$ . The sectors are stable and easily recognized for the oblate spheroids. However, for the spherical particles, stationary sectors are more difficult to achieve and could not be reliably reproduced.

Although the general bulk motion of the particles remains helical, the sector mode is distinct from the toroidal mode. Defining the general direction of the precessional motion as streamwise, it is seen that the particles on the upstream side of the crests are drawn into the bed, while on the downstream side particles emerge on the surface. The upstream particles have been exposed to air for a longer period and have dried, causing the dye to lose fluorescence. The upstream side of the crests thus appear darker than the downstream side, yielding the “rays” seen in Fig. 12. Also, in the sector mode, the secondary circulation roll near the wall that was characteristic of the unmodified toroidal mode of motion could not be observed.

As  $\omega$  is further increased to 26 Hz, the toroidal motion (without sectors or surface waves) is recovered. Unfortunately, the mechanical limitations of the apparatus did not allow testing at larger  $\omega$ .

## V. DISCUSSION

### A. Rotation of the particle bed in the horizontal plane

The direction of rotation of the particle bed in the horizontal plane is generally opposite to that of the center of the pan. This behavior is initially counter-intuitive, and explaining it requires a detailed understanding of the interplay between the bed motion, the pan orientation, and the horizontal and vertical components of the pan motion.

A crucial element for resolving this behavior is to determine the shape and motion of the zone of contact of the particle bed with the pan. Because the pan is tilted away from the vertical at all times during its motion, it seems likely that only a particular sector of the bed is in contact with the pan at any given time; and, that the angle at which maximum contact occurs between the bed and the pan rotates about the pan center at the same frequency  $\omega$  as the pan center itself. If this is true, at least two contributions to the mechanism of bed rotation can be envisioned:

(i) *Deflection by the pan surface:* Consider an element of the pan surface within the zone of contact between the pan and bed. At any given time, the normal to this surface element can be decomposed into vertical, radial, and tan-

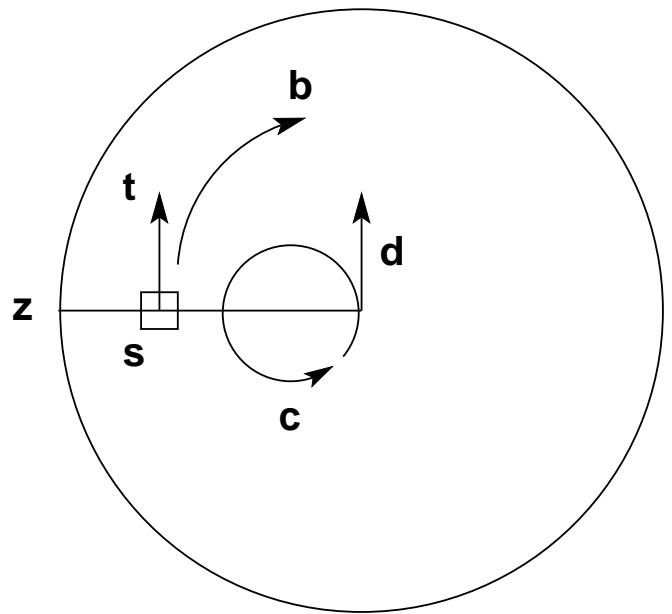


FIG. 13: Schematic illustration of scenarios for explaining direction of bed rotation. The large circle represents the edge of the pan as viewed from above.  $c$  is the circular trajectory of the centre of the pan as seen in the lab frame, while  $d$  is the instantaneous direction of motion of the pan centre at the moment depicted.  $s$  is a surface element of the pan bottom along the direction  $z$  of the zone of maximum contact between the pan and the bed. Scenario (i): If the vector  $t$  represents the tangential component of the normal to  $s$ , then particles will be deflected along  $t$ , leading to bed rotation in the direction  $b$ , opposite to  $c$ . Scenario (ii): If the vector  $t$  represents the tangential component of the velocity of  $s$ , then particles will be “dragged” in the direction of  $t$ , leading to bed rotation along  $b$ , again opposite to  $c$ .

gential components, defined with respect to a cylindrical coordinate system in the lab frame. Particles striking this surface element will tend to be deflected according to the orientation of the surface normal. In the absence of other mechanisms, a net rotational motion about the pan centre will occur if the direction of the tangential component remains constant. This will be true if (as assumed above) the zone of particle-bed contact rotates around the pan bottom at the same frequency as the pan itself precesses. The direction of this bed rotation will be independent of the rotational direction of the pan center, since it depends on the (presently unknown) location of the region of particle-bed contact. Hence, the bed could well be set into a rotational motion opposite to that of the pan center (Fig. 13).

(ii) *Entrainment by the pan surface:* Independent of the above mechanism, the effect of friction between the particles and the pan bottom should also be considered. As described in Section II, the pan bottom consists of a metal screen, and so is “rough” on the scale of the particles themselves. Consider the same surface element in the contact zone as discussed above, but instead of its



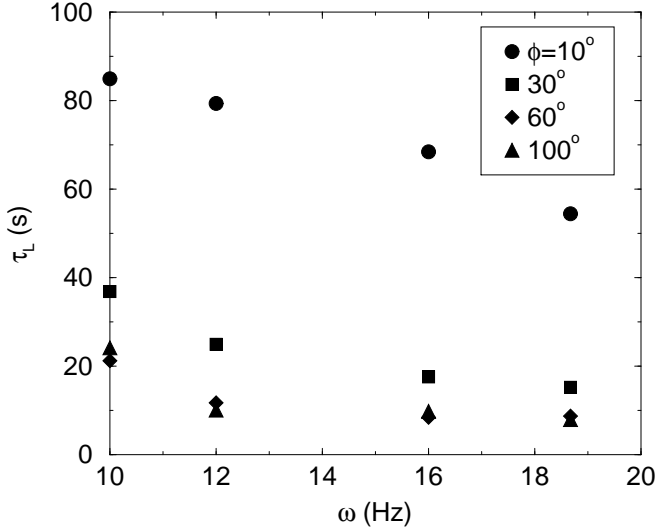


FIG. 14: A plot of the average lap time  $\tau_L$  in seconds.

orientation, consider its velocity vector decomposed into vertical, radial, and tangential components. This rough surface element will tend to transfer momentum to particles in contact with it according to the direction of its velocity. Analogous to the reasoning given above, particles in the contact zone will be subjected to a constant tangential surface velocity, yielding a net rotation of the bed about the pan center. Also as above, the direction of the resulting bed rotation will be independent of that of the pan center, and so it should be possible to establish conditions where these rotations would be in opposite in direction (Fig. 13).

Whatever the underlying mechanism, an explanation can be tested against the observed dependence of the motion on the control parameters. For example, the speed of rotation of the bed in the horizontal plane depends on the phase difference between the horizontal and vertical pan motions,  $\alpha_{xz}$ . For  $0^\circ < \alpha_{xz} < 180^\circ$ , the particles are observed to move in the direction opposite to that of the bed. However, as mentioned earlier, it is indeed possible to realize conditions where the bed rotates in the same direction as the pan, when  $\phi$  is changed such that  $\alpha_{xz} < 0^\circ$ .

In addition, the rotational speed of the bed in the horizontal plane increases with  $\omega$ . Furthermore, as shown in Fig. 14, the rotational speed is found to be greatest when  $\alpha_{xz} = 90^\circ$ , corresponding to  $\phi = 60^\circ$  (see Fig. 6).

Elucidation of these phenomena requires information on the (time-dependent) location of contact between the pan and the bed. This information is not available in the present measurements. These questions are being explored through further experiments, and through computer modelling.

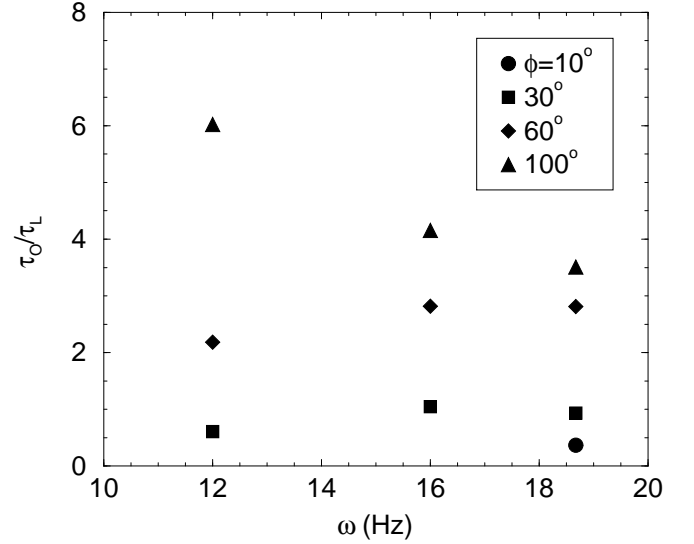


FIG. 15: A plot of the overs to lap ratio for the oblate spheroids.

## B. Radial motion of the particles

Understanding the radial motion of the particle bed also requires a careful consideration of the bed and pan motions. In the toroidal mode, the particles move along the bottom of the bed toward the wall, and then back toward the center of the pan along the top surface of the bed. It seems likely that the motion of particles near the pan bottom is due to their being entrained by the motion of the pan surface itself. The inward motion of particles on the bed surface, where the particle packing is looser, may be dominated by gravity-induced downward flow toward the bed center, where the bed depth is smallest. However, these possible explanations do not fully elucidate the origin of the toroidal shape adopted by the bed in this mode, and so further study of this behavior is needed.

The ratio of the rotational speed of the particle bed in the horizontal plane, to the radial speed is shown in Fig. 15. To measure this, the motion of color-tagged particles is observed in steady state. The average time  $\tau_L$  required for a tagged particle to complete one circuit (a “lap”) around the pan in the horizontal plane is measured; the average time  $\tau_O$  required for a tagged particle to complete one circuit (an “over”) from the center of the pan to the outside edge and back to the center is also measured. The ratio  $\tau_L/\tau_O$  is shown in Fig. 15.

In the heaping mode the radial motion is negligible, as indicated in Fig. 9. When the vertical acceleration is sufficiently high to fluidize the particles (i.e. the particles are not in continuous contact with the pan surface), the radial and horizontal rotational speeds of the particles are found to depend only on the phase difference between the horizontal and vertical pan motions. This is shown in Fig. 15: as  $\omega$  is increased,  $\tau_O/\tau_L$  approaches a constant

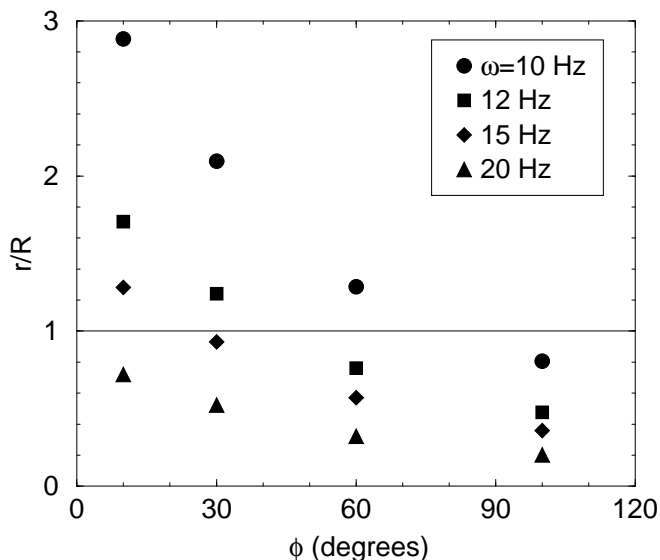


FIG. 16: Critical radius at which the vertical acceleration is  $g$  as a function of  $\phi$ .

value, which is a function of  $\phi$ .

### C. Critical acceleration and fluidization

The data in Fig. 5 are used to determine the critical radius, shown in Fig. 16, at which the maximum vertical acceleration exceeds  $g$ . For  $\phi = 10^\circ$  and  $\omega < 18$  Hz, the vertical acceleration is less than  $g$  and the particles at the bottom of the bed are constantly in contact with the pan surface. This is consistent with the radial motion of the particle bed being negligible, as indicated in Fig. 8. Based on the model motion in Eqs. 1-3, for  $\omega = 20$  Hz, the vertical acceleration exceeds  $g$  when  $r_p/R > 0.81$ . Under these conditions the toroidal motion is induced, in which case an overs-to-lap ratio could be clearly defined (Fig. 15). As  $\phi$  increases, the critical value of  $g$  occurs in the bed at smaller  $\omega$ , in agreement with the observations summarized in Fig. 8.

When the maximum vertical acceleration in the pan is less than  $g$ , the tilting motion of the pan induces only a

rotational motion of the bed in the horizontal plane, since the particles at the bed bottom remain more or less in constant contact with the pan surface and the net radial bed motion is zero. When the maximum acceleration exceeds  $g$ , the particles at the bottom of the bed are lifted above the pan surface, allowing a net radial displacement to be induced, and leading to the toroidal motion. Note that the toroidal mode is induced below the critical acceleration of  $1.2g$  reported for fluidization of granular matter in other studies [16, 17, 18]. For  $\phi > 30^\circ$  and  $\omega > 16$  Hz, the particle bed is fluidized over most of the pan area. This is the range of  $\omega$  in which the “wave” and “sector” modes are seen.

In their study of a deep bed of granular matter, Wassgren et al. [7] have shown that the bed undergoes a stage with an arched base, and during this stage, the bed moves out-of-phase with the container. A similar argument can be put forth for the circular bed in the present study. The motion that is imparted to the bed depends on the pan motion and the phase difference between the pan and the bed. When the bed moves out-of-phase with the pan, the point of next contact with the pan becomes a function of the pan motion. The instantaneous traces of the pan vertical displacement show period-doubling when the surface waves were observed in the particle bed. At every second cycle, the maximum upward vertical displacement is slightly less than that of the first cycle. The difference in amplitude decreases as the surface waves accelerate and the sectors eventually appear. The sectors may thus correspond to a standing wave.

Our observations are thus consistent with the existence of well defined states based on the frequency of the excitation. Computer simulations are currently underway to further elucidate the origin of the behavior described here [19].

### Acknowledgments

We thank Materials and Manufacturing Ontario and NSERC (Canada) for financial support. PHP also acknowledges support from the Canada Research Chairs program. We also acknowledge valuable discussions with K. Bevan., S. Fohanno, J.J. Drozd and E.B. Smith.

- 
- [1] H. M. Jaeger and S. R. Nagel, *Science* **255**, 1523 (1992).
  - [2] D. Bideau and J. Dodds, in *Physics of Granular Media*, (Les Houches Series, Nova Science Publishers, Commack, NY, 1991).
  - [3] *Granular Matter: An Interdisciplinary Approach*, edited by A. Mehta (Springer-Verlag, New York, 1994).
  - [4] H. M. Jaeger, S. R. Nagel, and R. P. Behringer, *Rev. Mod. Phys.* **68**, 1259 (1996).
  - [5] H. M. Jaeger, S. R. Nagel, and R. P. Behringer, *Phys. Today* **49**, No. 4, 32 (1996).
  - [6] P.-G. de Gennes, *Physica A*, **261**, 267-293 (1998).
  - [7] C. Wassgren, C. E. Brennen and M. L. Hunt, *Journal of Applied Mechanics (Trans ASME)*, **63**, 712-719 (1996).
  - [8] C. Bizon, M. D. Shattuck, J. B. Swift, W. D. McCormick and H. L. Swinney, *Physical Review Letters*, **80**, 57-60 (1998).
  - [9] S. G. K. Tennakoon and R. P. Behringer, *Physical Review Letters*, **81** (4), 794-797 (1998).
  - [10] M. A. Scherer, T. Mahr, A. Engel and I. Rehberg, *Physical Review E*, **58**, 6061-6072 (1998).
  - [11] D. V. Khakhar, J. J. McCarthy, and J. M. Ottino, *Physics of Fluids*, **9**, 3600-3614 (1997).

- [12] Y. Lan and A. D. Rosato, *Physics of Fluids*, **9**, 3615-3624 (1997). vibrated beds"
- [13] J. B. Knight, E. E. Ehrichs, V.Yu. Kuperman, J. K. Flint, H. M. Jaeger and S. R. Nagel, *Physical Review E*, **54**, 5726-5738 (1996).
- [14] S. G. K. Tennakoon, L. Kondic and R. P. Behringer, *Europhysics Letters*, **45** (4), 470-475 (1998).
- [15] C. Saluena, and T. Poschel, *The European Physical Journal E*, **1**, 55-59 (2001).
- [16] P. Evesque and J. Rajchenbach, *Physical Review Letters*, **62**, 44 (1989).
- [17] P. Evesque, E. Szmatala and J. P. Denis, *Europhys. Lett.*, **12**, 623 (1990).
- [18] P. Evesque, *Contemp. Phys.* **33**, 245 (1992).
- [19] O. Baran, J.J. Drozd, P. Sistla, R.J. Martinuzzi and P.H. Poole, preprint (2002).